Asian Journal of Chemistry; Vol. 37, No. 7 (2025), 1743-1752

ASIAN JOURNAL OF CHEMISTRY

https://doi.org/10.14233/ajchem.2025.33974

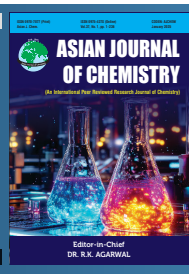

Investigation of Structural, Optical and Luminescent Properties of Zinc Sulfide Quantum Dots under the Influence of Acoustic Shockwaves

K. VIJAYAKUMAR, R. YOGA INDRA ENIYA and B. VIGNEASHWARI*

Department of Physics, Government Arts College for Men, Krishnagiri-635001, India

*Corresponding author: E-mail: vigneashwari@gmail.com

Received: 2 May 2025; *Accepted*: 20 June 2025; *Published online*: 30 June 2025; AJC-22051

Zinc sulfide (ZnS) is a promising semiconducting material with its applications in optoelectronics and solar cell technologies. In this research, ZnS QDs were synthesized by co-precipitation technique. The powder X-ray diffraction analysis and high-resolution transmission electron microscopy (HRTEM) revealed that as-synthesized ZnS possess a cubic structure in the quantum dot (QD) regime. Furthermore, the compositional purity of as-prepared sample were analyzed using energy dispersive X-ray Analysis (EDAX). The prepared material was exposed to acoustic shockwaves in a series of 200 and 400 shock pulses using a semi-automatic Reddy tube, an instrument manufactured indigenously to generate acoustic shockwaves having a Mach number of 1.5, a transient temperature and pressure of 520 K and 0.59 MPa. The experimental findings of the present work state that ZnS QDs with a cubic structure are studied under the acoustic shockwave-treated conditions and the effect of high-pressure created on the structural parameters was systematically studied using the PXRD technique. The optical properties were studied using UV-Vis DRS analysis shows a noticeable shift in the absorption wavelength along with the tunable optical band gap energy (E_g). The photoluminescence (PL) spectra showed an increase in the PL intensity at 400 shock-loaded conditions, demonstrating the improved crystallinity and reduction in defects. Finally, the structure-property relationship of ZnS with respect to the strength of shockwave exposure was discussed in detail. The obtained experimental results suggest that ZnS QDs can be suitable for optoelectronics, luminescent devices and durable shockwave-resistant solar energy harvesting systems.

Keywords: Zinc sulfide, Quantum dots, PXRD, HRTEM, Shockwaves, UV-Vis-DRS, Photoluminescence.

INTRODUCTION

In recent years, shockwave-influenced phase transitions of nanomaterials have peaked as an outstanding field and obtained such interest that it opens the pathways for discovering many materials for potential applications, including piezoelectric, dielectric and ferroelectric materials [1,2]. The impact of shockwaves on materials has been performed by identifying the properties of crystals under shock-loaded conditions. Moreover, the phase transitions such as crystalline to amorphous transitions and *vice-versa* are well documented [3-6]. Acoustic-shockwave influences reversible phase transitions and researchers paid attention for achieving reversibility under dynamic shock-loaded conditions. At high temperatures and high pressures, the switchable phase transitions of nanomaterials have potential usage in sensor applications [7,8].

Tuning the physical properties of nanomaterials is a part of shockwave research, which has gained interest globally in the past few decades. It fulfills the requirement of stable nanomaterials, which is used in aerospace applications. Moreover, engineering the properties of nanomaterials under the influence of shockwaves would provide intense growth of promising stable materials. At dynamic shock-loaded conditions, one can understand the stability of materials that cannot be noticed in ambient conditions. There is a huge demand for highly stable materials but the nanomaterials at extreme conditions such as high temperature, pressure, energy irradiations and shockwaves. Most of the nanomaterials fail due to the instability of structures even though they are deserved at ambient conditions. Hence, shockwaves fulfill the requirement of potentially stable nanomaterials for electronic devices in aerospace applications. The impact of bulk and nanocrystalline materials for studying the structural dynamics under high pressure shockwaves has been documented [9-14].

The transition of anatase-TiO_2 to rutile-TiO_2 under dynamic shock-loading conditions using a free-piston powered shock

tube was also reported in the literature [15,16]. The structural stability of α-Fe_2O_3 nanoparticles, which resulted in the degradation of crystallinity concerning the number of shock pulses, has been well documented [17]. Many materials such as CeO_2 [18], ZnO [19], CoO NPs [20], NiO NPs [21] have exhibited highly stable crystallographic structures under the dynamic shockwaves. On those queues, ferrite materials and metal oxides were investigated for the structural and magnetic properties and exhibited interesting results under shock-loaded conditions [21-24]. Based on the recent research, on metal sulfides with the experiments obtained on dynamic shockwave impact are reported with the layered materials such as tungsten disulfide (WS_2), molybdenum disulfide (MoS_2) under the impact of shockwaves showed the considerable reduction in inter-planar spacing and increment in shear deformations concerning the number of shock pulses [25] Acoustic shockwave on zinc sulfide nanoparticles upto 150 shock pulses as reported by Aswathappa *et al.* [26].

Over the past few decades, efforts have been made to synthesize highly fluorescent quantum dot (QDs). The quantum confinement effect results in the narrow emission spectra for the excitation wavelengths in a wide range. Such properties have attracted interest in the applications of imaging and biological fluore-scence. In the past years, the ZnS QDs have attained the spot-light significance for research in order to improve the optical and structural properties [27-35]. Researchers reported that ZnS QDs having a particle size of about 2.7 nm with zinc blende have transformed into wurtzite structure at 400 ºC [36]. In addition, irradiation of acoustic shockwaves can strongly improve and affect the properties of ZnS QDs, such as displacement of atoms and formation of defects or by restoring the original crystal structure. Furthermore, optical properties can be influenced by exposure to acoustic shockwaves. Therefore, high pressure induced by acoustic shockwaves to the ZnS QDs can play an important role in improving the quality of such materials. Herein, a simple chemical precipitation method was used to synthesize ZnS QDs and the experiment on the impact of shockwaves of 200 and 400 shock pulses were carried out. Interestingly, a stable cubic (B3) structure coexisted with a hexagonal (B4) structure after the shockwave exposure was witnessed, whereas the optical properties were altered, confirmed through UV-visible DRS analysis and fluorescence spectroscopy for widening its applications in diverse fields. Therefore, understanding the shockwave-induced tuning of optical properties could lead to the evolution of efficient technological solutions, since there were only a few reports on the systematic examination of ZnS under extreme conditions. In this present work, an acoustic shockwave-loaded experiment for cubic zinc blende ZnS QDs was carried out. Surfing through the literature, no experiment on ZnS QDs at extreme conditions with acoustic shockwaves has been reported; hence, an acoustic shockwave-loaded ZnS QDs experiment with a transient pressure of 0.59 MPa was undertaken and their impacts were also discussed.

EXPERIMENTAL

ZnS QDs synthesis procedure: In this experiment, all the chemical agents were purchased from Merck and were used without additional purification. Zinc acetate ($Zn(CH_2COO)_2$) and sodium sulfide nonahydrate were used as precursors for zinc and sulfur sources. In order to prepare the solutions, deionized water was used as solvent, to ensure the highest purity of experimental procedures. The precipitation method was adopted for synthesizing ZnS QDs. Initially, $Zn(CH_2COO)_2$ (1 M) and $Na_2S{\cdot}9H_2O$ (1 M) were dissolved separately in 50 mL deionized water water at the ambient temperature. The solutions were magnetically stirred for 1.5 h in order to get a homogenous mixture, upon the dropwise addition of sodium sulfide and stirred at 400 rpm for 6 h, which led to a pale-white colour solution. The obtained solution was kept undisturbed until the occurrence of precipitation. The resulting precipitates were washed and centrifuged multiple times with water and ethanol. The collected precipitates were air-dried at 80 ºC for 2 h. Thereafter, the sample was dried for 1 h at 120 ºC to obtain a fine powder, which was used for further characterization and also for acoustic shockwave loading experiments.

Acoustic shockwave loading approach: The acoustic shockwaves were developed by a tabletop-pressure-driven shock tube. Fig. 1 represents the automatic Reddy tube, which is capable of producing supersonic shock waves. It comprises three sections namely, the driven, driver and diaphragm sections. Atmospheric air (O_2) was used to generate shockwaves, which was supplied by a tabletop air compressor with the capacity of 8-bar pressure storage. The driven and driver sections are segregated by the diaphragm section. A 180 GSM carbonless paper was used as a diaphragm, which is ruptured at a critical pressure and the shockwaves are generated with the help of

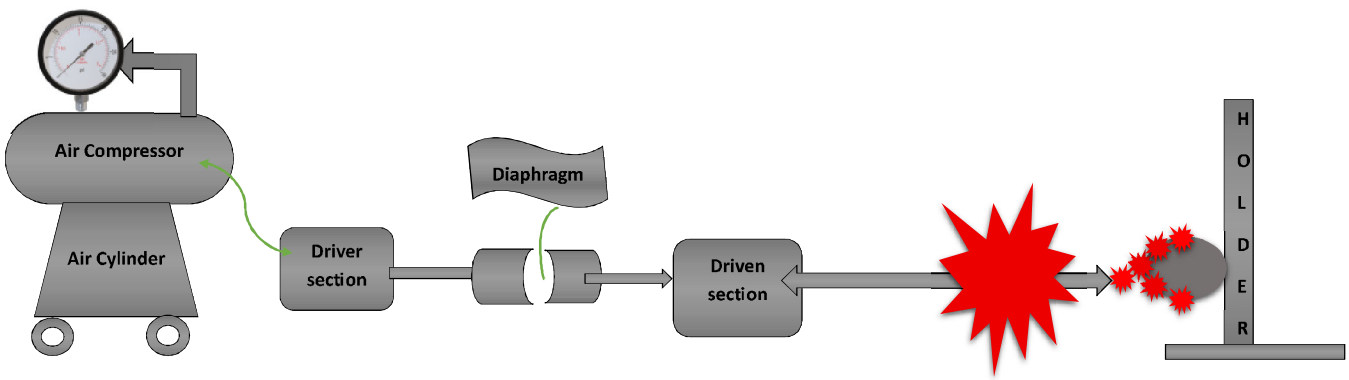

Fig. 1. Representation of acoustic shockloading technique set-up

compressed air. The shockwaves travel along the driven section and burst on the sample placed in the sample holder, which is placed 1 cm away from the driven section.

The acoustic shockwaves of each have a Mach number of 1.5 with 0.59 MPa and 520 K as the transient pressure and temperature [37], respectively. In this experiment, 3 samples of the same proportions were selected and one sample among them was kept as an unshocked sample and the other two samples were fed with 200 and 400 doses of shock pulses in regular time intervals.

Instrumentation: Powder X-ray diffraction (PXRD) [benchtop Bruker D2 phaser powder X-ray diffractometer, Cu*K*α was used as a source of X-rays of wavelength 1.5406 Å with a step size of ± 0.044º] analysis was carried out for both unshocked and shockwave treated ZnS. High-resolution transmission electron microscope (HRTEM) [JEOL-3010], selected area electron diffraction (SAED) and energy dispersive X-ray analysis (EDAX) analyses were performed to understand the structural properties of as-prepared (unshocked) ZnS QDs. An ultraviolet-visible diffuse reflectance [UV-Vis DRS using JASCO UV-Vis-NIR (V-770, Serial No. A012061801) spectrophotometer and a fluorescence spectrophotometer [Perkin-Elmer Model-LS45] was used to study the optical properties.

RESULTS AND DISCUSSION

Structural analysis of unshocked ZnS QDs: The P-XRD pattern of the as-synthesized zinc sulfide was recorded within the range of 20º to 80º for 2θ (º) as shown in Fig. 2. The obtained PXRD pattern was analyzed and peaks for zinc sulfide (ZnS) was cross-verified with JCPDS card no. 05-0566, which showed a good agreement with face-centered cubic structure with single phase ZnS without impurities. The major peaks were positioned with corresponding Miller indices (*hkl*) of (111), (220) and (311) planes, respectively. PXRD profiles of as-prepared ZnS indicate a single phase with $F\bar{4}3m$ space group, which represents that the as-synthesized ZnS has a fcc structure and has symmetry along axis rotation mirror plane and it is centrosymmetric. For cubic structures, the lattice parameters are a = b = c = 5.345 Å and the interfacial angles are α = β = γ = 90º,

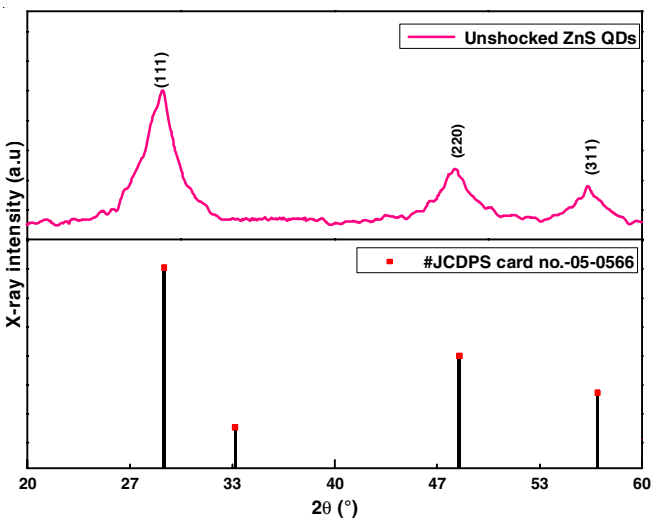

Fig. 2. PXRD pattern of unshocked ZnS QDs

respectively. On applying, the Debye-Scherrer's formula, the crystallite size of ZnS was found to be 2.38 nm, which was within the excitonic Bohr radius (r_B = 2.5 nm). The broadening observed in the diffraction peaks indicates the formation of ZnS of small-sized nanocrystals. The average crystallite size and PXRD peak broadening correlate with each other and it shows that the as-synthesized ZnS are within the quantum confinement regime, referred to as quantum dots (QDs).

HRTEM studies: The HRTEM images of as-prepared ZnS QDs show the presence of agglomerates as shown in Fig. 3a. From Fig. 3b, it can be clearly seen that the as-prepared sample consists of a large number of particles having an average particle diameter ranging from 10 to 12 nm as represented in Fig. 3c, which appeared due to the accumulation of QDs. The average particle size of the as-prepared sample was calculated using the ImageJ software. It was noticed that the particle size of ZnS observed from the HRTEM micrograph is larger than the crystallite size of ZnS obtained from the Debye-Scherrer formula. This is because each particle has ultra-fine crystallites whose sizes were determined using the PXRD technique. Fig. 3d depicts the selected area electron diffraction (SAED) pattern of ZnS QDs, which shows the formation of concentric rings instead of spots due to the random orientation of the crystallites related to diffraction from the planes of the ZnS crystallites.

Also, from the SAED pattern, the three strong rings are indexed, which corresponds to (111), (220) and (311) planes of the cubic structure of ZnS QDs. The obtained results suggest that the as-synthesized ZnS QDs are polycrystalline and are in good agreement and blended with the PXRD results. Fig. 3e reveals the energy dispersive X-ray analysis (EDAX) of as-synthesized ZnS QDs. The purity and composition of ZnS QDs were confirmed and the existence of zinc (Zn) and sulfur (S) in the proper ratio was observed. The other peaks in the EDAX spectrum might have been originated during the data acquisition, respectively.

PXRD analysis of shockwave-treated samples: Under the ambient conditions, ZnS crystallizes into two crystal structures *i.e.*, B3 and B4. However, the cubic crystal structure of ZnS was obtained for unshocked sample. In addition, the PXRD patterns of 200 and 400 shockwave loaded samples clearly represents the formation of a cubic structure with an additional tiny diffraction peak at 30.68º which matches with #JCPDS card no. 89-2942 having a hexagonal structure with the space group $P6_3mc$. The new peak appeared due to the shockwave treatment (Fig. 4). Furthermore, leading to atomic rearrangement in the crystal lattice by breaking of weaker bonds, causing the lattice distortion, which was induced due to the impact of shockwaves [38]. The lattice distortion has influenced the material's structure and thus led to variation in the lattice parameters [39]. The obtained results show that there was no peak vanishing observed at shockloaded conditions. Remarkably, the cubic phase remained stable at 200 and 400 shock pulses. The traces of hexagonal structure started emerging at 200 shockwave-treated conditions and found to be stable even up to 400 shocked conditions. Similar kinds of high phase stability materials have been found under the exposure of acoustic shockwaves [19,21]. To get the deep insights about the structural stability of cubic

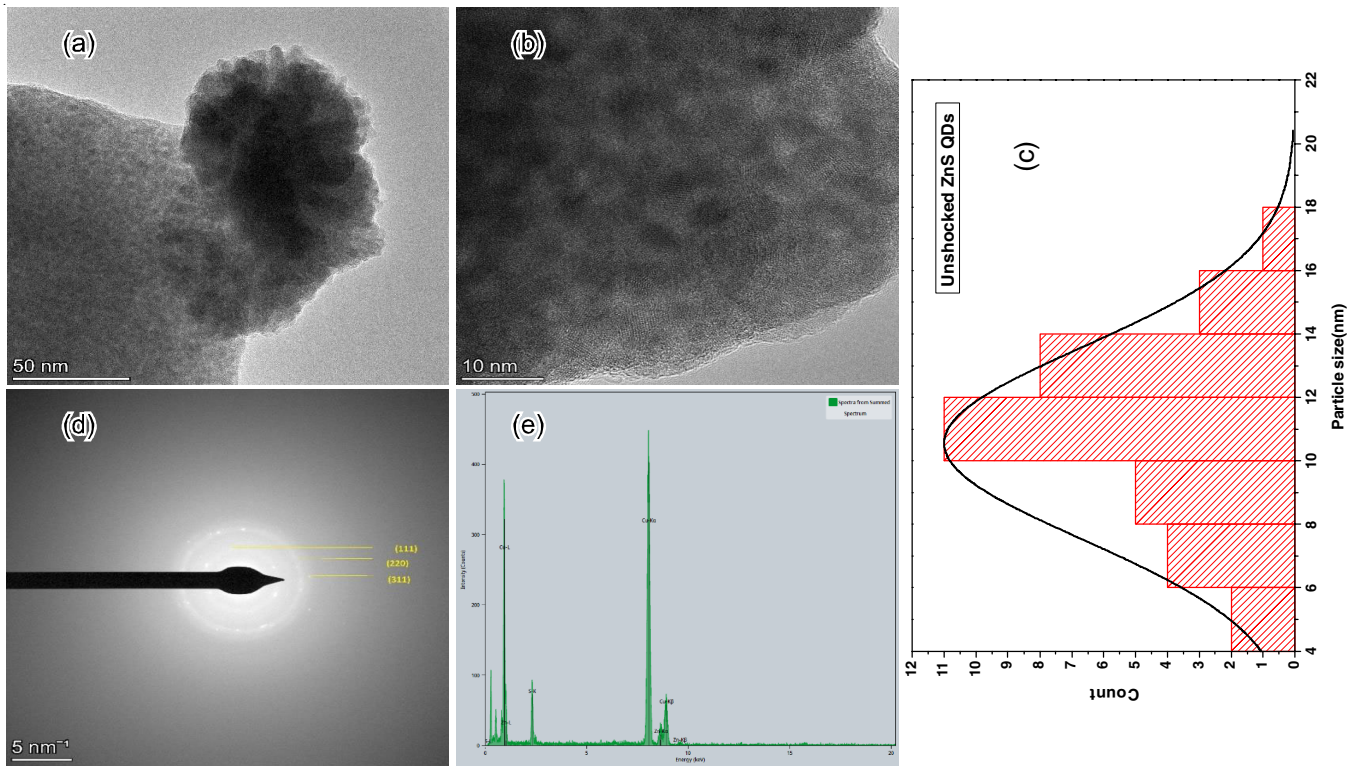

Fig. 3. (a) TEM image, (b) HRTEM micrograph, (c) average particle distribution histogram, (d) SAED pattern and (e) EDAX spectrum of unshocked ZnS QDS

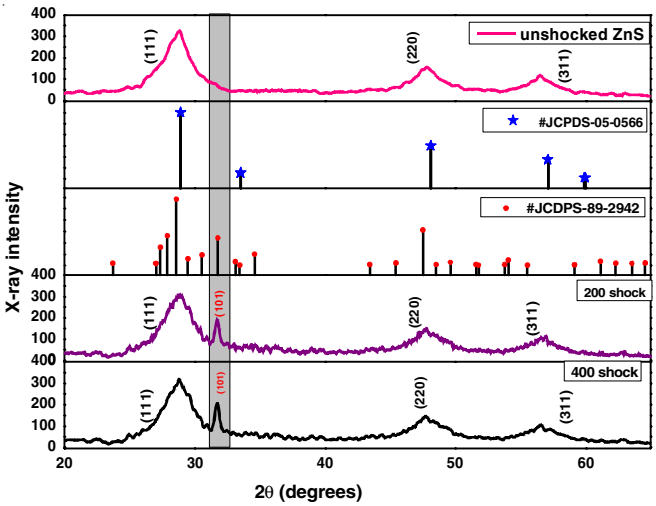

Fig. 4. Powder X-ray diffraction pattern of unshocked and shockwave-treated ZnS

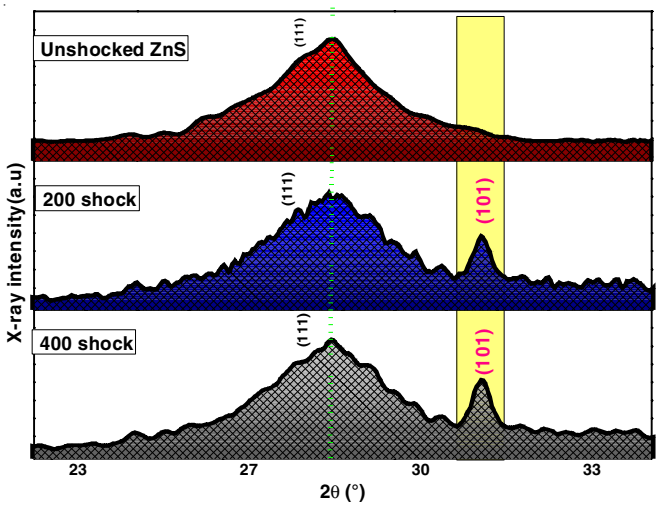

Fig. 5. PXRD pattern of zoomed-in (111), (101) planes for unshocked and shocked ZnS

phase of the unshocked and shocked ZnS, the magnified version of the most prominent PXRD plane (111) and (101) are shown in Fig. 5. The average crystallite size of the test samples was determined to be 5.28 nm and 5.45 nm for the 200 and 400 shock-loaded samples, respectively.

The lattice strain (ε) of ZnS before and after shockwave exposure were calculated using the following relation:

$$\varepsilon = \frac{\beta}{4\tan\theta}$$

Dislocation density of ZnS before and after shockwave exposure were estimated using the following equation:

$$\delta = \frac{1}{D^2}$$

where D denotes the crystallite size, which was derived using the Debye-Scherrer formula.

Fig. 6 shows the variation plot of crystallite size and lattice strain and *versus* number of shockpulses. It illustrates that an increase in the crystallite size was noticed with the reduction in lattice strain and dislocation density at the shock-loaded conditions which are tabulated in Table-1. The decrease in lattice strain and dislocation density with the increased crystallite size shows the reduction in grain boundaries, crystal defects

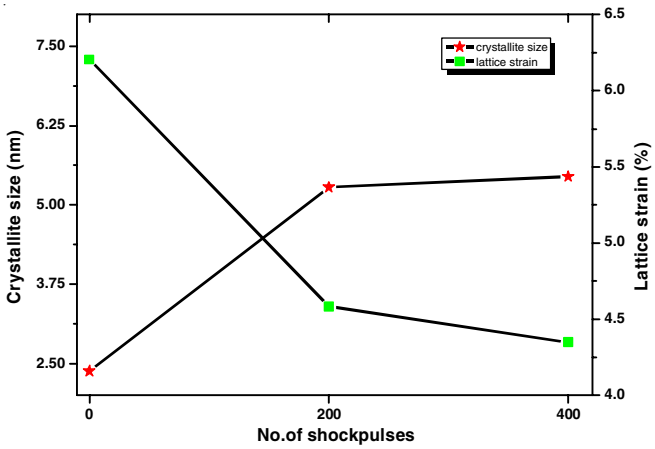

Fig. 6. Variation plot of number of shock pulses *versus* crystallite size (nm) and lattice strain (%)

TABLE-1
PXRD PARAMETERS OF UNSHOCKED AND SHOCK TREATED ZnS

Test conditions	D (nm)	Dislocation density (m^2)	Lattice strain (%)	d-spacing (Å) of (111) plane
0 shock pulses	2.38	21.680	6.205	3.425
200 shock pulses	5.28	14.725	4.583	3.362
400 shock pulses	5.45	13.412	4.349	3.298

and lattice imperfections [40,41]. As observed in Fig. 5, the appearance of a new peak at (101) is due to shockwave-induced structural distortion and structural reorientation [42,43]. Consequently, the intensity of PXRD peaks sharpens in the plane (101) leading to an increase in crystallite size which results in the improvement of crystallinity of ZnS under the impact of 200 and 400 shock pulses.

To investigate whether the lattice imperfections are present in the shock-treated ZnS, the calculations of lattice parameters and strain from PXRD pattern were performed. Moreover, unit cell volume and lattice parameters were calculated before and after shocked conditions using UNITCELL software [44]. Moreover, on the observations of PXRD of profiles of unshocked and shockwave-loaded samples, it is clear that the volume of the unit cell and the lattice parameters are slightly decreased compared to the unshocked conditions, which is directly related to lattice contraction due to the impact of shock pulses [45].

Furthermore, the decrease in unit cell volume and the values of lattice parameters shows the compression caused by the shockwaves, which made the bonds to compress and alter the atomic positions and thus inducing phase transition in the shockwave-treated samples. The variation plot clearly explains the corresponding changes that occurred during the impact of shockwaves which led to fluctuation in crystallite size [46], which caused the breakage and fusion of grain boundaries accompanying the crystal lattice to experience dynamic recrystallization process leading to rearrange the atoms within the crystal lattice. Also, it was observed that at shocked conditions, the B3-ZnS structure had tried to restructure itself with the hexagonal (B4) pattern of ZnS, but the phase transition process was incomplete at 200 and 400 shocked conditions. As reported in the literature [47], the ZnS NPs can modify the crystallographic nature easily when compared to particles in the macroscale. At 400 ºC, ZnS NPs transform from zinc blende to hexagonal (wurtzite) as reported in [47]. The cubic (B3) structure remained unmodified at the shocked conditions which confirms the high structural stability of cubic-ZnS under the acoustic shockwaves. The demonstrated structural stability might be due to the high bond strength of Zn and S, respectively. The B3 and B4 phases coexisted as a mixed phase at shock-loaded conditions. In other studies, upon high pressure, the mixed phases of B3 and B4 were observed [48]. According to the static pressure studies of ZnS, both phases retained their crystallographic characteristics up to 11 GPa.

While comparing the crystallographic lattice parameters of B3 and B4 structures, the hexagonal (B4) structure has an axial length of the *c*-axis (6.188 Å) that is longer than that of the *a*-axis (3.777 Å). According to the observations, compressibility values and lattice parameters, the hexagonal (B4) crystal structure could easily experience lattice deformations when compared to the cubic (B3) structure under high-pressure conditions [49,50] as illustrated in Table-1. From Fig. 4, the PXRD pattern, it is evident that FWHM values of the B4 structure have undergone a considerable variation in FWHM and variation in the peak shape under the shock-loaded conditions whereas the cubic (B3) structure has sustained similar FWHM values and also, no change in the shape of peaks was observed under the shocked conditions. Fig. 7 shows the FWHM plots of hexagonal and cubic structures *versus* the number of shock pulses.

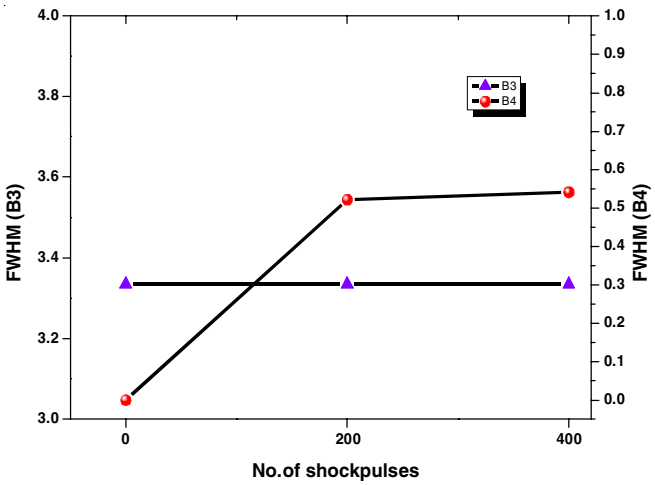

Fig. 7. FWHM values of B3 and B4 structures against the number of shock pulses of 0.59 MPa

Optical properties of unshocked and shockwave-loaded ZnS QDs

UV-Vis DRS studies: The UV-Vis- DRS spectra before and after loading shock pulses are shown in Fig. 8, which were recorded within the wavelength range between 200 to 800 nm, respectively. Before being subjected to acoustic shock pulses, ZnS QDs had an absorption at 301 nm, relatively a blue shift as compared to bulk cubic ZnS (340 nm) [51]. The absorption peak at a lower wavelength region can be related to the mean diameter of the particles with the smaller size of unshocked

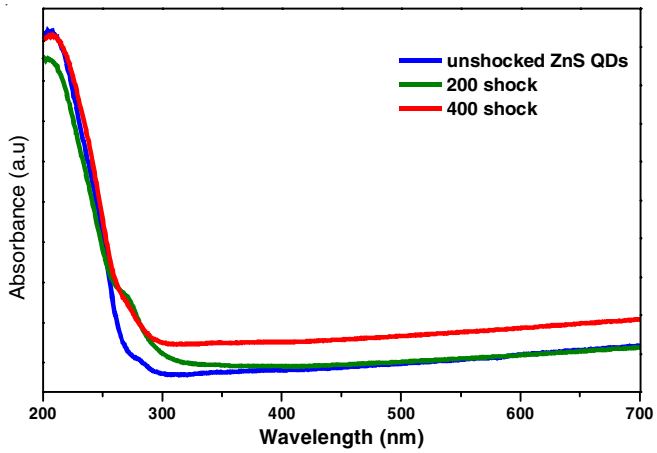

Fig. 8. UV-Vis DRS spectra of unshocked and shock-loaded ZnS

ZnS QDs. The obtained results show the effect of quantum size effect (QSE) *i.e.*, quantum confinement effect. This effect determines the shift of optical absorption edge towards higher energies with decreasing particle size in the direct bandgap semiconductor nanoparticles; thus, explaining the UV-vis blue-shift effect [52-54]. The findings also demonstrated that the electronic properties significantly change as the dimension of particle becomes either comparable to or less than that of the Bohr radius of an exciton (r_B) and so a blue shift in the absorption wavelength can be observed. Analogous to the quantum confinement effect, electrons and holes in the Fermi energy level are spatially confined by the potential barrier of the surface. Appropriately to confine the electrons and holes, the bandgap energy effectively increases, thereby the energy required for the lowest-energy optical transition from the valence band (VB) to conduction band (CB) will increase [55]. It can be associated with self-activated defect centers related to zinc vacancies [56]. After loading 200 shock pulses, the absorption edge shifted to 314 nm and for 400 doses of shock pulses it further shifted to 323 nm, respectively.

From the obtained UV-Vis DRS spectra, the ZnS before and after shocked conditions efficiently absorbs the UV radiation in the lower wavelength range, which makes it a significant choice for applications that require sensitivity to UV light [57]. From the optical absorption spectra, the bandgap energy of ZnS before and after shockwave treatment was calculated using the following relation:

$$E_g = h\nu = \frac{hc}{\lambda}$$

where E_g represents the optical bandgap energy; h is Planck's constant; c denotes the velocity of light; and λ corresponds to the maximum absorption wavelength of unshocked and shocked ZnS. The corresponding optical bandgap energy of unshocked ZnS QDs was 3.98 eV, which is found to be higher than compared to bulk ZnS (3.70 eV). The Bohr excitonic radius (r_B), is about 2.5 nm for cubic ZnS [58]. The size of particles can be estimated from the absorption peak using Brus' effective model [58,59] is given as follows:

$$\Delta E_g = \frac{h^2\pi^2}{2R^2}\left[\frac{1}{m_e m_o} + \frac{1}{m_h m_o}\right]$$

where ΔE_g represents the difference in the E_g for ZnS QDs and bulk ZnS; h denotes the reduced Planck's constant; m_e is the effective mass of electron in the conduction band (CB); m_h is the hole in the valence band (VB); for ZnS (m_e = 0.34, m_h = 0.5), m_0 corresponds to the rest mass of electron [60]. The calculated values are in good agreement with the obtained PXRD results for unshocked and shocked conditions.

As a result of acoustic shockwaves, ZnS experiences extreme pressure and temperature due to rapid compression and the atoms as well as the electronic states can be modified within the material. The optical bandgap energy of 200 and 400 acoustic shock-treated ZnS is 3.94 eV and 3.83 eV, which clearly indicates the red shift in absorption edges as compared to unshocked conditions. It was observed that the decrease in optical band gap energy is explained by the rise in band tails energy of localized states, as reported earlier [61]. As stated in the investigation of PXRD results, the observable shifting in absorption edges which attributed to the lattice compression and also the effects of the size of the nanoparticles [62-64]. Furthermore, the Kubelka-Munk relation was used to calculate the direct band gap for unshocked and shocked ZnS. Fig. 9 represents the obtained band gap plots, whereby the estimated bandgap energies were identified to be 3.98 eV, 3.94 eV and 3.83 eV for 0, 200 and 400 shocked conditions, respectively. The impact of shockwave alters the electronic structure and also enhances the crystallinity and reduces the lattice defects, which causes the variation in the light absorption properties and thus results in a new absorption peak [65,66]. The optical properties could be influenced by various imperfections like point dislocations, distortions and point defects. In addition, the disordered arrangement of the atoms of a crystal lattice could impact the optical properties [67,68]. The energy bandgap between CB and VB reduces due to decreased interatomic distance (*d*-spacing), which leads to the modifications of Fermi energy levels and thus results in reduced bandgap energies [69] at 200 and 400 shocked conditions as compared to unshocked conditions.

These circumstances also create the localized states within the bandgap, which require higher energy for electron transi-

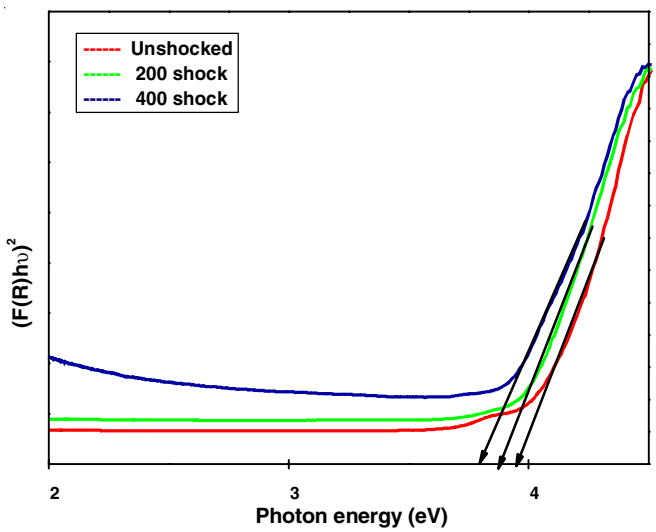

Fig. 9. Bandgap energy plot using Kubelka-Munk relation for unshocked and shockwave-loaded ZnS

tions from CB to VB, thereby causing changes in the electronic properties and reducing the energy band gap [70,71] with respect to the number of shock pulses of 0.59 MPa. When ZnS QDs were subjected to the acoustic shock pulses, the red shift was observed due to shockwave-induced lattice distortion [71-73], which correlated with PXRD analysis. Furthermore, the band gap of 200 and 400 shock-loaded ZnS is decreased as than that of unshocked ZnS; the influence of shock pulses might cause rapid compression, thus leading the crystal lattice to expand or contract and thus rearranging the atoms from their original positions within the crystal lattice [74]. Contraction in the lattice brings the neighbouring atoms closer to each other. This reduces the lattice parameters and spacing between the atoms and thus leading to increased overlapping of the electronic orbitals. Thereby, the energy difference between CB and VB decreases, since less energy is required for electronic transitions, thus giving rise to reduced bandgap energy. Under the impact of acoustic shockwaves, ZnS after shockwave exposure was found to increase, the bandgap energy decreased with an increase in crystallite size since the bandgap energy is dependent on the crystallite size of the material [75]. Furthermore, from the investigations, there was tunability in bandgap energy at the shocked conditions, which further confirms the phase transition and so the decreased bandgap energy and therefore, it can be used to improve the efficiency in energy conversion devices. The acoustic shockwaves induce the defects or disorders and the lattice contraction influences the absorbance rate, which has a great impact in the optical properties and thus resulting in the decreased bandgap energy [76]. Many researchers have reported that the optical bandgap energy is mainly associated with the size of the nanoparticles apart from the phase transformation process [77,78]. Therefore, under the shockwave exposure, the present study tuning of the material's bandgap energy is achieved. Also, the obtained results from UV-DRS analysis it validates that high pressure created by acoustic shock pulses causes the narrowing of bandgap energy due to lattice contraction in the crystal lattice [69] of ZnS QDs. The tunability in the bandgap of ZnS QDs under shocked conditions finds its usage in the field of solar cells, optoelectronics, *etc.* [79-81]. The variation plot of crystallite size and bandgap energy *versus* the number of shock pulses is presented in Fig. 10.

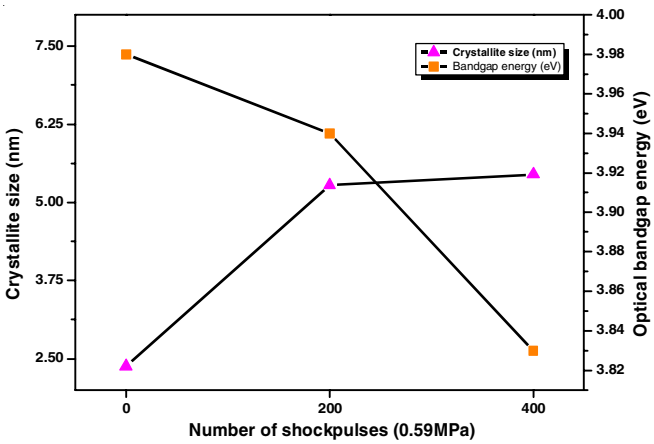

Fig. 10. Variation plot of crystallite size and bandgap *versus* number of shock pulses

Photoluminescence: Fig. 11 shows the photoluminescence (PL) spectra of unshocked and shocked ZnS were recorded using 300 nm as excitation wavelength. The emission peak of ZnS was positioned at 329 nm before the exposure to shockwaves; this value was well-corroborated with the literature [82]. When ZnS was subjected to 200 and 400 shock pulses, there was no alteration in the PL peak position. Remarkably, the intensity of PL peaks tends to change when increasing the strength of shockwaves. The change in PL intensity of shockwave-treated ZnS corresponds to the improved crystallinity. This justifies that the improvement in crystallinity increases the efficiency of the radiative recombination rate, as corroborated by combining increased crystallinity with stronger emission characteristics in semiconductors [83].

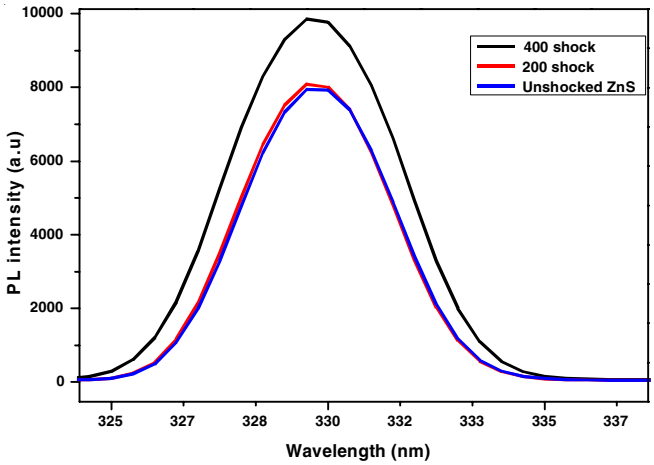

Fig. 11. Photoluminescence spectra of unshocked and shocked ZnS

Fig. 12 represents the PL spectra within the wavelength region between 400 to 550 nm for shocked and unshocked ZnS. It is visible that PL emission bands were obtained, which are asymmetric and broadened with multiple emission peaks, indicating the involvement of different luminescent centres in the radiative process [84].

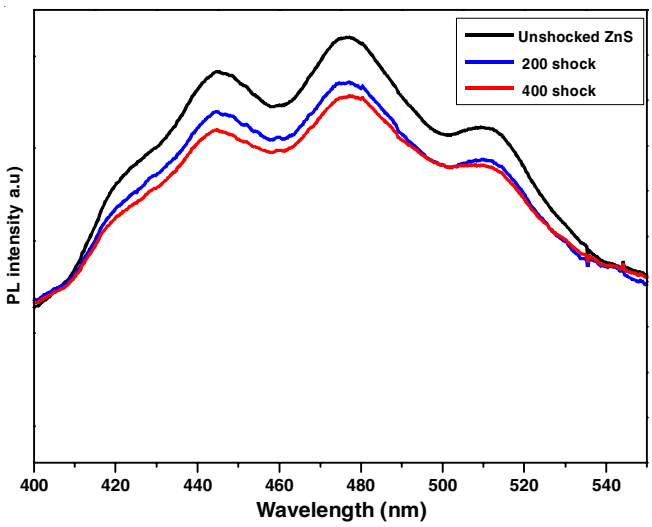

Fig. 12. Magnified version of the PL spectrum of unshocked and shock-treated ZnS

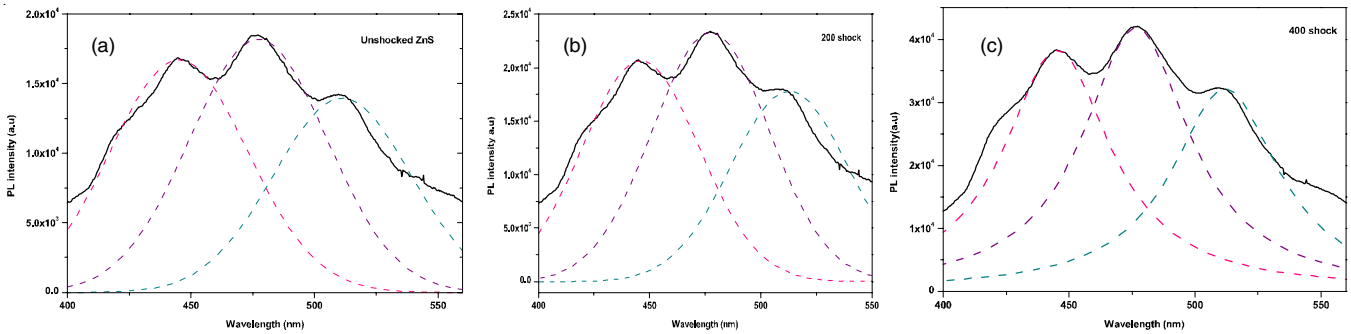

Fig. 13. Gaussian fitting curves of PL spectra for (a)unshocked ZnS, (b) 200 shocked ZnS and (c) 400 shocked ZnS

Fig. 13 represents the Gaussian peak fittings of the PL spectra of unshocked and shocked conditions, where the colour dashed lines show the individual Gaussian curves and the darkened black solid lines denotes the experimentally obtained PL emission band. Clearly, it was found that the PL spectra of all the samples have three emission peaks lying in the visible region of the electromagnetic spectrum and are well-matched with the literature [84]. The peaks were positioned at 445, 476 and 520 nm for all the samples, respectively. Many researchers have claimed that ZnS has near band-edge emission at ~340 nm, a self-activated emission band at 420 nm and a green emission band at ~535 nm [85]. Furthermore, the emission peak attributed at 445 nm; a blue emission peak which is associated with defect related emission in the ZnS host, the peak situated at 476 nm is corresponding to dangling sulfur bonds at the interface of ZnS and the PL peak observed at 520 nm was assigned to elemental sulfur species on the surface of ZnS [86,87].

The increase in the PL emission band intensities is due to the impact of shockwaves, which caused excitation and recombination of excitons as reported earlier [38]. The alteration in the PL emission intensity could be due to shockwave-induced increment in the molecular interactions, which modifies the electron states and thus results in enhancement or reduction in the PL intensity [88]. PL intensity is directly proportional to the crystallite size as claimed by the other research groups. As the crystallite size increases, defect density decreases which leads to reduced lattice strain in the shockwave loaded conditions. Furthermore, it results in more efficient recombination rate of excitons, which ultimately increases the PL intensity [89]. It could be demonstrated that PL intensity is not only related to the concentration of defects but also it has a great influence on structural and electronic factors induced by the acoustic shockwaves. These findings highlight the potential of ZnS for device-based applications under extreme-pressure and temperature conditions which enable its suitability in solar cell technologies and optoelectronics.

Conclusion

In summary, zinc sulfide (ZnS) QDs were synthesized and subjected to acoustic shockwaves of 0.59 MPa in a series of 200 and 400 shock pulses, which were compared with as-prepared ZnS QDs for their structural, optical and luminescence properties. Based on the structural analysis point of view, the cubic (B3) structure of ZnS coexists with the hexagonal (B4) structure, which confirms the structural stability of the cubic-ZnS structure under extreme conditions. The optical properties show that the reduction in optical bandgap energies as compared to unshocked conditions enables the possibility of tuning the bandgap from 3.98 eV to 3.83 eV under high pressure. The luminescence properties were analyzed by PL spectral analysis, which shows broad emission in the ultraviolet and as well as visible regions, respectively. Since ZnS is used in flat panel displays, optoelectronics, as a window layer in thin-film photovoltaics and optical imaging. This study suggests that ZnS has a high tendency to withstand extreme conditions. This research thus opens a new pathway into optimizing and fine-tuning the optoelectronic properties of ZnS QDs, for their usage in efficient solar energy harvesting systems.

CONFLICT OF INTEREST

The authors declare that there is no conflict of interests regarding the publication of this article.

REFERENCES

1. N. Mayilswamy, A. Krishnan, M. Mundhada, H. Deodhar, G. Joshi and B. Kandasubramanian, *Ind. Eng. Chem. Res.*, **62**, 6584 (2023); https://doi.org/10.1021/acs.iecr.3c00837
2. L.S. Chinke, I.S. Sandhu, D.R. Saroha and P.S. Alegaonkar, *ACS Appl. Nano Mater.*, **1**, 6027 (2018); https://doi.org/10.1021/acsanm.8b01061
3. S.C. Gupta, *Bull. Mater. Sci.*, **22**, 295 (1999).
4. A. Sivakumar, S.S.J. Dhas, P. Sivaprakash, A.I. Almansour, R.S. Kumar, N. Arumugam, S. Arumugam and S.A.M.B. Dhas, *New J. Chem.*, **45**, 16529 (2021); https://doi.org/10.1039/D1NJ02974F
5. A. Sivakumar, S.S.J. Dhas, S. Chakraborty, R.S. Kumar, A.I. Almansour, N. Arumugam and S.A.M.B. Dhas, *J. Phys. Chem. C*, **126**, 3194 (2022); https://doi.org/10.1021/acs.jpcc.1c09411
6. A. Sivakumar, S.S.J. Dhas, J. Thirupathy, K.P.J. Reddy, R.S. Kumar, A.I. Almansour, S. Chakraborty and S.A.M.B. Dhas, *New J. Chem.*, **46**, 5091 (2022); https://doi.org/10.1039/D2NJ00129B
7. Z. Liu, L. Zhang and D. Sun, *Chem. Commun.*, **56**, 9416 (2020); https://doi.org/10.1039/D0CC03197F
8. L. Zhou, P.-P. Shi, X. Zheng, F.-J. Geng, Q. Ye and D.-W. Fu, *Chem. Commun.*, **54**, 13111 (2018); https://doi.org/10.1039/C8CC07311B
9. K. Kadau, T.C. Germann, P.S. Lomdahl and B.L. Holian, *Science*, **296**, 1681 (2002); https://doi.org/10.1126/science.1070375
10. W. Xuan, R. Pow, N. Watfa, Q. Zheng, A.J. Surman, D.-L. Long and L. Cronin, *J. Am. Chem. Soc.*, **141**, 1242 (2019); https://doi.org/10.1021/jacs.8b09750
11. Z. Su, W.L. Shaw, Y.-R. Miao, S. You, D.D. Dlott and K.S. Suslick, *J. Am. Chem. Soc.*, **139**, 4619 (2017); https://doi.org/10.1021/jacs.6b12956

12. N.K. Reddy, V. Jayaram, E. Arunan, Y.-B. Kwon, W.J. Moon and K.P.J. Reddy, *Diamond Rel. Mater.*, **35**, 53 (2013); https://doi.org/10.1016/j.diamond.2013.03.005
13. A. Sivakumar, S.R. Devi, S.S.J. Dhas, R.M. Kumar, K.K. Bharathi and S.A.M.B. Dhas, *Cryst. Growth Des.*, **20**, 7111 (2020); https://doi.org/10.1021/acs.cgd.0c00214
14. A. Sivakumar, S.S.J. Dhas and S.A.M.B. Dhas, *J. Mater. Sci. Mater. Electron.*, **31**, 13704 (2020); https://doi.org/10.1007/s10854-020-03928-0
15. V. Jayaram, P. Singh, K.P.J. Reddy, *Adv. Ceram. Sci. Eng.*, **2**, 40 (2013).
16. S. Kalaiarasi, A. Sivakumar, S.A.M.B. Dhas and M. Jose, *Mater. Lett.*, **219**, 72 (2018); https://doi.org/10.1016/j.matlet.2018.02.064
17. A. Rita, A. Sivakumar, M. Jose and S.A.M.B. Dhas, *Mater. Res. Express*, **6**, 095035 (2019); https://doi.org/10.1088/2053-1591/ab2eba
18. V. Jayaram, A. Gupta and K.P.J. Reddy, *J. Adv. Ceram.*, **3**, 297 (2014); https://doi.org/10.1007/s40145-014-0121-1
19. M. Devika, N.K. Reddy, V. Jayaram and K.P.J. Reddy, *Adv. Mater. Lett.*, **8**, 398 (2017); https://doi.org/10.5185/amlett.2017.6890
20. A. Sivakumar, S. Soundarya, S.S.J. Dhas, K.K. Bharathi, S.A.M.B. Dhas, *J. Phys. Chem. C*, **124**, 10755 (2020); https://doi.org/10.1021/acs.jpcc.0c02146
21. A. Rita, A. Sivakumar and S.A.M.B. Dhas, *J. Supercond. Nov. Magn.*, **33**, 1845 (2020); https://doi.org/10.1007/s10948-020-05435-z
22. V. Mowlika, C.S. Naveen, A.R. Phani, A. Sivakumar, S.A.M.B. Dhas and R. Robert, *J. Mater. Sci. Mater. Electron.*, **31**, 14851 (2020); https://doi.org/10.1007/s10854-020-04047-6
23. A. Sivakumar, S.S.J. Dhas and S.A.M.B. Dhas, *Solid State Sci.*, **107**, 106340 (2020); https://doi.org/10.1016/j.solidstatesciences.2020.106340
24. K. Showrilu, C. Jyothirmai, A.R.N.L. Sirisha, A. Sivakumar, S.S.J. Dhas and S.A.M.B. Dhas , *J. Mater. Sci. Mater. Electron.*, **32**, 3903 (2021); https://doi.org/10.1007/s10854-020-05133-5
25. K. Vasu, H.S.S.R. Matte, S.N. Shirodkar, V. Jayaram, K.P.J. Reddy, U.V. Waghmare and C.N.R. Rao, *Chem. Phys. Lett.*, **582**, 105 (2013); https://doi.org/10.1016/j.cplett.2013.07.044
26. S. Aswathappa, L. Dai, S.J.D. Sathiyadhas, M.B.D.S. Amalapushpam, M. Vijayan, R.S. Kumar and A.I. Almansour, *Ceram. Int.*, **50**, 7418 (2024); https://doi.org/10.1016/j.ceramint.2023.12.028
27. E.K. Goharshadi, R. Mehrkhah and P. Nancarrow, *Mater. Sci. Semicond. Process.*, **16**, 356 (2013); https://doi.org/10.1016/j.mssp.2012.09.012
28. K.T. Al-Rasoul, I.M. Ibrahim, I.M. Ali and R.M. Al-Haddad, *Int. J. Sci. Technol. Res.*, **3**, 213 (2014).
29. M. Madkour, T. Salih, F. Al-Sagheer and A. Bumajdad, *Opt. Mater. Express*, **6**, 2857 (2016); https://doi.org/10.1364/OME.6.002857
30. C. Ippen, T. Greco, Y. Kim, J. Kim, M.S. Oh, C.J. Han and A. Wedel, *Org. Electron.*, **15**, 126 (2014); https://doi.org/10.1016/j.orgel.2013.11.003
31. W. Zhang, S. Ding, W. Zhuang, D. Wu, P. Liu, X. Qu, H. Liu, H. Yang, Z. Wu, K. Wang and X.W. Sun, *Adv. Funct. Mater.*, **30**, 2005303 (2020); https://doi.org/10.1002/adfm.202005303
32. H. Kumar, A. Kumari and R.R. Singh, *Opt. Mater.*, **69**, 23 (2017); https://doi.org/10.1016/j.optmat.2017.04.009
33. R. Zhang, Y. Wang, M. Jia, J. Xu and E. Pan, *Appl. Surf. Sci.*, **437**, 375 (2018); https://doi.org/10.1016/j.apsusc.2017.12.110
34. T.I. Chanu, D. Samanta, A. Tiwari and S. Chatterjee, *Appl. Surf. Sci.*, **391**, 548 (2017); https://doi.org/10.1016/j.apsusc.2016.05.045
35. K. Komal, P. Shikha and T.S. Kang, *New J. Chem.*, **41**, 7407 (2017); https://doi.org/10.1039/C7NJ01373F
36. S.B. Qadri, E.F. Skelton, D. Hsu, A.D. Dinsmore, J. Yang, H.F. Gray and B.R. Ratna, *Phys. Rev. B Condens. Matter*, **60**, 9191 (1999); https://doi.org/10.1103/PhysRevB.60.9191
37. S. Oviya, F.I. Maria Bincy, R.S. Kumar, P. Kannappan, I. Kim and S.A.M. Britto Dhas, *Mater. Chem. Phys.*, **333**, 130287 (2025); https://doi.org/10.1016/j.matchemphys.2024.130287
38. F.I.M. Bincy, S. Oviya, R.S. Kumar, P. Kanappan, I. kim and S.A.M.B. Dhas, *J. Mater. Sci.*, **59**, 7044 (2024); https://doi.org/10.1007/s10853-024-09574-9
39. S.L. Morelhão, S.W. Kycia, S. Netzke, C.I. Fornari, P.H.O. Rappl and E. Abramof, *J. Phys. Chem. C*, **123**, 24818 (2019); https://doi.org/10.1021/acs.jpcc.9b05377
40. C.O. Ehi-Eromosele, B.I. Ita and E.E.J. Iweala, *J. Sol-Gel Sci. Technol.*, **76**, 298 (2015); https://doi.org/10.1007/s10971-015-3777-2
41. B. Azhdar, *J. Exp. Nanosci.*, **18**, 2276278 (2023); https://doi.org/10.1080/17458080.2023.2276278
42. Y. Sun, L. Wang, Y. Liu and Y. Ren, *Small*, **11**, 300 (2015); https://doi.org/10.1002/smll.201400892
43. P.H. Le, C.-N. Liao, C.W. Luo and J. Leu, *J. Alloys Compd.*, **615**, 546 (2014); https://doi.org/10.1016/j.jallcom.2014.07.018
44. A. Sivakumar, S.S.J. Dhas, S. Balachandar and S.A.M.B. Dhas, *J. Electron. Mater.*, **48**, 7868 (2019); https://doi.org/10.1007/s11664-019-07605-9
45. Z.Y. Liu, J. Li, J.F. Zhang, J. Li, P.T. Yang, S. Zhang, G.F. Chen, Y. Uwatoko, H.X. Yang, Y. Sui, K. Liu and J.-G. Cheng, *NPJ Quantum Mater.*, **6**, 90 (2021); https://doi.org/10.1038/s41535-021-00393-8
46. A. Rita, A. Sivakumar and S.A.M.B. Dhas, *J. Nanostruct. Chem.*, **9**, 225 (2019); https://doi.org/10.1007/s40097-019-00313-0
47. X. Fang, T. Zhai, U.K. Gautam, L. Li, L. Wu, Y. Bando and D. Golberg, *Prog. Mater. Sci.*, **56**, 175 (2011); https://doi.org/10.1016/j.pmatsci.2010.10.001
48. S.B. Qadri, E.F. Skelton, A.D. Dinsmore, J.Z. Hu, W.J. Kim, C. Nelson and B.R. Ratna, *J. Appl. Phys.*, **89**, 115 (2001); https://doi.org/10.1063/1.1328066
49. H. Zhao, W. Liu, J. Zhu, X. Shen, L. Xiong, Y. Li, X. Li, J. Liu, R. Wang, C. Jin and R. Yu, *High Press. Res.*, **35**, 9 (2015); https://doi.org/10.1080/08957959.2014.996562
50. Y. Ji, L. Guo, H. Xu, J. Liu, X. Li, Y. Li, Z. Wu and P. Simon, *Phys. Status Solidi, A Appl. Res.*, **198**, 210 (2003); https://doi.org/10.1002/pssa.200306450
51. I. Yu, T. Isobe and M. Senna, *J. Phys. Chem. Solids*, **57**, 373 (1996); https://doi.org/10.1016/0022-3697(95)00285-5
52. Y.L. Li, Y.H. Wang and J. Yun, *Guangpuxue Yu Guangpu Fenxi*, **27**, 1890 (2007).
53. X.W. Zhao, S. Komuro, S. Fujita, H. Isshiki, Y. Aoyagi and T. Sugano, *Mater. Sci. Eng. B*, **51**, 154 (1998); https://doi.org/10.1016/S0921-5107(97)00250-X
54. J. Borah, J. Barman and K.C. Sarma, *Chalcogenide Lett.*, **5**, 201 (2008).
55. A.P. Alivisatos, *Nature*, **271**, 933 (1996); https://doi.org/10.1126/science.271.5251.933
56. S.H.A. Allehyani, R. Seoudi, D.A. Said, A.R. Lashin and A. Abouelsayed, *J. Electr. Mater.*, **44**, 4227 (2015); https://doi.org/10.1007/s11664-015-3974-3
57. A. Rai, P. Phogat, Shreya, R. Jha and S. Singh, *MATEC Web Conf.*, **393**, 01011 (2024); https://doi.org/10.1051/matecconf/202439301011
58. H. Tang, G. Xu, L. Weng, L. Pan and L. Wang, *Acta Mater.*, **52**, 1489 (2004); https://doi.org/10.1016/j.actamat.2003.11.030
59. Y. Li, Y. Ding, Y. Zhang and Y. Qian, *J. Phys. Chem. Solids*, **60**, 13 (1999); https://doi.org/10.1016/S0022-3697(98)00247-9
60. A.E. Raevskaya, A.V. Korzhak, A.L. Stroyuk and S.Y. Kuchmii, *Theor. Exp. Chem.*, **41**, 111 (2005); https://doi.org/10.1007/s11237-005-0029-5
61. A.M. Al-Baradi, M.M. El-Nahass, M.M.A. El-Raheem, A.A. Atta and A.M. Hassanien, *Radiat. Phys. Chem.*, **103**, 227 (2014); https://doi.org/10.1016/j.radphyschem.2014.05.055
62. Z. Li, B. Liu, S. Yu, J. Wang, Q. Li, B. Zou, T. Cui, Z. Liu, Z. Chen and J. Liu, *J. Phys. Chem. C*, **115**, 357 (2011); https://doi.org/10.1021/jp107304v

63. Z. Li, J. Wang, B. Liu and J. Liu, *J. Phys. Chem. C*, **120**, 781 (2016); https://doi.org/10.1021/acs.jpcc.5b11195
64. V.D. Mote and B.N. Dole, *J. Mater. Sci. Mater. Electron.*, **32**, 420 (2021); https://doi.org/10.1007/s10854-020-04790-w
65. S. Atroshenko, A. Divakov, Y. Meshcheryakov and N. Naumova, *Mater. Sci. Forum*, **794**, 755 (2014); https://doi.org/10.4028/www.scientific.net/MSF.794-796.755
66. D. Raabe, Recovery and Recrystallization: Phenomena, Physics, Models, Simulation, In: Physical Metallurgy, Elsevier edn. 5, pp. 2291–2397 (2014).
67. A.A. El-Fadl and A.M. Nashaat, *Radiat. Eff. Defects Solids*, **170**, 863 (2015); https://doi.org/10.1080/10420150.2015.1123259
68. M.A. Gaffar and A. Abu El-Fadl, *Cryst. Res. Technol.*, **34**, 915 (1999); https://doi.org/10.1002/(SICI)1521-4079(199908)34:7<915::AID-CRAT915>3.0.CO;2-W
69. F. Wang, M. Tan, C. Li, C. Niu, X. Zhao, *Org. Electron.*, **67**, 89 (2019); https://doi.org/10.1016/j.orgel.2019.01.003
70. R. Sreekumar, R. Jayakrishnan, C. Sudha Kartha, K.P. Vijayakumar, S.A. Khan and D.K. Avasthi, *J. Appl. Phys.*, **103**, 23709 (2008); https://doi.org/10.1063/1.2829812
71. N. Puri, K.R. Gupta, N.C. Mehra, R.P. Tandon and A.K. Mahapatro, *Integr. Ferroelectr.*, **184**, 9 (2017); https://doi.org/10.1080/10584587.2017.1368630
72. X. Ren, X. Yan, A.S. Ahmad, H. Cheng, Y. Li, Y. Zhao, L. Wang and S. Wang, *J. Phys. Chem. C*, **123**, 15204 (2019); https://doi.org/10.1021/acs.jpcc.9b02854
73. X. Ren, X. Yan, A.S. Ahmad, H. Cheng, Y. Li, Y. Zhao, L. Wang and S. Wang, *Chalcogenide Lett.*, **5**, 297 (2008); https://doi.org/10.1021/acs.jpcc.9b02854
74. Y. Kanemitsu, Y. Ishida, I. Nakada and H. Kuroda, *Appl. Phys. Lett.*, **48**, 209 (1986); https://doi.org/10.1063/1.96797
75. M.N. Siddique, T. Ali, A. Ahmed and P. Tripathi, *Nano-Object.*, **16**, 156 (2018); https://doi.org/10.1016/j.nanoso.2018.06.001
76. A. Sivakumar, A. Saranraj, S. Sahaya Jude Dhas, M. Jose and S.A. Martin Britto Dhas, *Opt. Eng.*, **58**, 077104 (2019); https://doi.org/10.1117/1.OE.58.7.077104
77. L. Li, J. Hu, W. Yang and A.P. Alivisatos, *Nano Lett.*, **1**, 349 (2001); https://doi.org/10.1021/nl015559r
78. O.L. Stroyuk, V.M. Dzhagan, V.V. Shvalagin and S.Y. Kuchmiy, *J. Phys. Chem. C*, **114**, 220 (2010); https://doi.org/10.1021/jp908879h
79. H.C. Liao, M.C. Wu, M.H. Jao, C.M. Chuang, Y.F. Chen and W.F. Su, *CrystEngComm*, **14**, 3645 (2012); https://doi.org/10.1039/c2ce06154f
80. W.M. Linhart, S.J. Zelewski, P. Scharoch, F. Dybala and R. Kudrawiec, *J. Mater. Chem. C Mater. Opt. Electron. Devices*, **9**, 13733 (2021); https://doi.org/10.1039/D1TC03625D
81. Z. Amara, M. Khadraoui, R. Miloua, M.N. Amroun and K. Sahraoui, *J. Optoelectron. Adv. Mater.*, **22**, 163 (2020).
82. X.T. Zhou, P.-S.G. Kim, T.K. Sham and S.T. Lee, *J. Appl. Phys.*, **98**, 024312 (2005); https://doi.org/10.1063/1.1988974
83. S. Naseem Shah, S. Rizwan Ali, S. Qaseem, Yasmeen Bibi, U. Majeed, S. Masood, *J Nanoscope*, **3**, 1 (2022); https://doi.org/10.52700/jn.v3i1
84. A.K. Kole and P. Kumbhakar, *Appl. Nanosci.*, **2**, 15 (2012); https://doi.org/10.1007/s13204-011-0036-x
85. C. Ye, X. Fang, G. Li and L. Zhang, *Appl. Phys. Lett.*, **85**, 3035 (2004); https://doi.org/10.1063/1.1807018
86. C.S. Tiwary, P. Kumbhakar, A.K. Mondal and A.K. Mitra, *Phys. Status Solidi., A Appl. Mater. Sci.*, **207**, 1874 (2010); https://doi.org/10.1002/pssa.200925341
87. D. Denzler, M. Olschewski and K. Sattler, *J. Appl. Phys.*, **84**, 2841 (1998); https://doi.org/10.1063/1.368425
88. K.A. Bhabu, J. Theerthagiri, J. Madhavan, T. Balu, G. Muralidharan and T.R. Rajasekaran, *J. Mater. Sci. Mater. Electron.*, **27**, 10980 (2016); https://doi.org/10.1007/s10854-016-5214-x
89. C. Mrabet, M. Ben Amor, A. Boukhachem, M. Amlouk and T. Manoubi, *Ceram. Int.*, **42**, 5963 (2016); https://doi.org/10.1016/j.ceramint.2015.12.144